J. Plasma Phys. (2023), *vol*. 89, 905890416
Published by Cambridge University Press

doi:10.1017/S0022377823000831

Non-locality of ion reflection at the shock front: dependence on the shock angle

Michael Gedalin †

Department of Physics, Ben-Gurion University of the Negev, Beer-Sheva, Israel

(Received 16 April 2023; revised 24 July 2023; accepted 25 July 2023)

In typical heliospheric collisionless shocks most of the mass, momentum and energy are carried by ions. Therefore, the shock structure should be most affected by ions. With the increase of the Mach number, ion reflection becomes more and more important, and reflected ions participate in shaping the shock profile. Ion reflection at the collisionless shock is a non-local process: the reflected–transmitted ions re-enter the shock front far from the reflection point. The direction and the magnitude of this shift depend on the shock angle. The distance between the reflection point and the re-entry point is of the order of the upstream ion convective gyroradius and exceeds the shock width. The non-locality of ion reflection may have implications for shock rippling since reflected ions may carry perturbations along the shock front.

Key words: space plasma physics

1. Introduction

In typical heliospheric collisionless shocks most of the mass, momentum and energy are carried by ions. Therefore, the shock structure should be most affected by ions. In sufficiently low-Mach-number shocks, all or almost all ions cross the shock from the upstream region to the downstream region and proceed further without return (directly transmitted ions). In these shocks ion heating is due to the gyration of directly transmitted ions (Gedalin 1997, 2021) and the downstream magnetic structure, including moderate overshoot, is due to the non-gyrotropy of the downstream ion distributions. This non-gyrotropy causes spatially quasi-periodic variations of the total, dynamic and kinetic, pressure of ions, and corresponding variations of the magnetic pressure in the opposite phase (Balikhin *et al.* 2008; Gedalin, Friedman & Balikhin 2015). With the increase of the Mach number, ion reflection becomes progressively more and more important, and the contribution of reflected–transmitted ions to ion heating is substantial (Sckopke *et al.* 1983; Scudder *et al.* 1986; Sckopke *et al.* 1990). For a long time, ion reflection was described in the convenient but physically not feasible approximation of specular reflection (Gosling *et al.* 1982). Specular reflection assumes that an ion with the bulk flow velocity is instantly reflected by a potential wall in such a way that the normal component of the ion velocity flips while the others do not change. The above description implies working in the normal

† Email address for correspondence: gedalin@bgu.ac.il

incidence frame (NIF), in which the incident plasma flow velocity (upstream velocity) is along the shock normal. The specular reflection approximation has been used for years and is still often used for observational estimate of the shock speed and conversion of time in the spacecraft frame to a spatial coordinate system (Gosling & Thomsen 1985). In reality, ions should enter the shock transition where the magnetic field increases and the cross-shock potential builds up (Morse 1973; Formisano 1982; Schwartz *et al.* 1987, 1988; Dimmock *et al.* 2012; Cohen *et al.* 2019) before the normal component of their velocity drops to zero and changes sign. It was shown, theoretically and observationally (Sckopke *et al.* 1983; Gedalin 1996, 2016) that ion reflection is essentially non-specular. This has been shown already in early simulations (Burgess, Wilkinson & Schwartz 1989) but remained unnoticed. It was shown recently (Balikhin & Gedalin 2022) that the widely used expression of Gosling & Thomsen (1985) overestimates the actual excursion of the reflected ions along the shock normal by a factor of two. This has to be taken into account when converting spacecraft measurements of the magnetic field as a function of time to the spatial dependence of the magnetic field.

Present focus in the studies of ion reflection by shocks is mainly on the energies the ions can achieve (see, e.g. Trattner *et al.* 2023), on the ion phase space holes (see, e.g. Wang *et al.* 2022), on the observations of multiple ion phase space holes as a rippling signature (Johlander *et al.* 2018) and on the role of reflected ions in rippling formation (Lowe & Burgess 2003; Moullard *et al.* 2006; Burgess & Scholer 2007; Johlander *et al.* 2016; Gingell *et al.* 2017; Omidi *et al.* 2021). The motion of the reflected ions is not studied in detail, which is understandable, since neither observations nor simulations follow individual ion trajectories but measure ions appearing at a certain position and/or time, without precise knowledge of where they came from.

Shock structure depends, in general, on the angle θ_{Bn} between the shock normal and the upstream magnetic field vector. Most quasi-perpendicular shocks, $\theta_{Bn} > 45^\circ$, have a clear structure where the steepest magnetic field increase, the ramp, is followed by an overshoot, undershoot and possibly more coherent magnetic oscillations (Bale *et al.* 2005). Quasi-parallel shocks, $\theta_{Bn} < 45^\circ$, often have a less regular and more extended transition with no clear ramp and overshoot (Burgess *et al.* 2005). This is, however, not a rule. In many cases, a quasi-parallel shock has a clear magnetic profile with the same structural elements as in quasi-perpendicular shocks. An example is shown in figure 1. This shock crossing is taken from the database of the Magnetospheric MultiScale (MMS) shock crossings (Lalti *et al.* 2022). The shock angle is determined in the database as $\theta_{Bn} \approx 32^\circ$, well within the quasi-parallel range. The black line shows the magnetic field magnitude measured in the fast mode, 16 vectors per sec. The high temporal resolution of measurements reveals plenty of fluctuations/small-scale structure. The thin red line shows the magnetic profile with the small-scale fluctuations and structure removed. The removal is done by applying wavelet transform with the Daubechies 10 wavelet, removing the 7 finest levels of the total 13 levels and applying the inverse transform. The denoised profile exhibits the basic elements of the shock profile of a typical quasi-perpendicular shock. Note that the wavelet transform smooths the transition from the foot to the ramp. In what follows, our discussion refers to the shocks with a well-defined structure (after removal of small-scale fluctuations/structure), like the one shown in figure 1.

After being reflected, ions gyrate in the upstream magnetic and electric field ahead of the shock transition before coming to the shock again and crossing it toward downstream, thus becoming a reflected–transmitted ion population. The distance between the reflection point and the re-entry point may well exceed the width of the shock transition. Thus, the whole process is non-local in space. This non-locality is known and was used for explanation of the foot formation (Woods 1971; Leroy *et al.* 1982) as well as for the mechanism of shock

https://doi.org/10.1017/S0022377823000831 Published online by Cambridge University Press

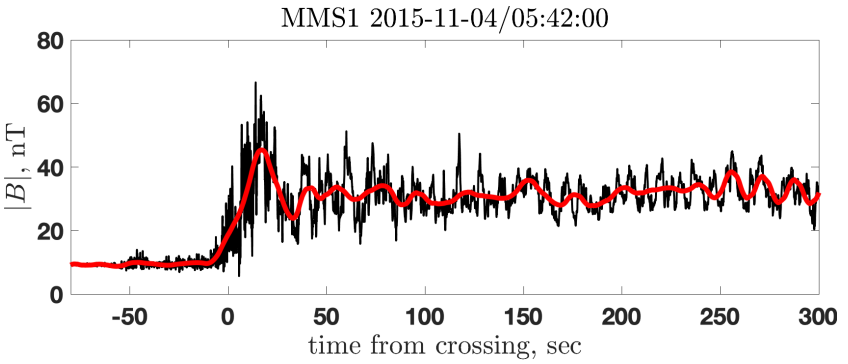

FIGURE 1. A quasi-parallel shock measured by MMS 1. The shock angle is $\theta_{Bn} \approx 32^{\circ}$. The black line shows the magnetic field magnitude measured in the fast mode, 16 vectors per sec. The high temporal resolution of measurements reveals plenty of fluctuations/small-scale structure. The thick red line shows the magnetic profile with the small-scale fluctuations and structure removed. The removal is done by applying wavelet transform with the Daubechies 10 wavelet, removing the 7 finest levels of the total 13 levels and applying the inverse transform.

drift acceleration by multiple reflection (see, e.g. Zank *et al.* 1996). In both cases only the reflected ion motion in the direction of the NIF motional electric field is of interest. The motional electric field is in the direction perpendicular to the shock normal and to the upstream magnetic field vector. However, the reflected ions move also in the direction of the magnetic field. If the shock is planar and stationary, there seem to be no other implications of the non-locality, because of the translational invariance along the shock front. However, at large Mach numbers, shocks are expected to become rippled (Lowe & Burgess 2003; Moullard *et al.* 2006; Burgess & Scholer 2007; Lobzin *et al.* 2008; Ofman & Gedalin 2013; Burgess *et al.* 2016; Johlander *et al.* 2016; Gingell *et al.* 2017; Johlander *et al.* 2018; Omidi *et al.* 2021). If this is the case, an ion which is reflected at some position at the shock front re-enters the shock transition, which may have different parameters. On the other hand, if a perturbation occurs at some shock position, ions, which are reflected at this position, convey this perturbation to a quite another position on the shock front. In the absence of translational invariance on a rippled surface, this may cause a stabilizing effect or instability. Thus, knowledge of the dependence of the shift of a reflected ion between the reflection and re-entry points is important to understanding of rippling development and for interpretation of observations. The latest hybrid simulations (Burgess *et al.* 2016; Omidi *et al.* 2021) suggest that rippling is generated by the instability between the reflected ions and the background plasma, and that the direction and speed of ripple propagation is determined by the reflected ion velocity in the turnaround point. The direction of the shift between the reflection point and the re-entry point is consistent with this velocity. In the present paper, we use test particle analysis in a model shock to study the non-locality of ion reflection and corresponding ion distributions within the shock transition. Such test particle analyses are actually an extension of the theory on systems where the equations of motion cannot be solved analytically. Modelling of the shock profile is a necessary part of any theoretical investigation and allows us also to extract information from observations (Gedalin *et al.* 2022). Although test particle analysis is sometimes considered inferior compared with sophisticated self-particle simulations, it has the advantage of controlling each parameter separately, which allows us to determine multi-parameter dependencies. The spatial resolution is not limited by any grid cell size and each particle trajectory can be easily followed. The method has already demonstrated its efficiency. As an example, it has

https://doi.org/10.1017/S0022377823000831 Published online by Cambridge University Press

been used to explain the downstream magnetic oscillations as a response to non-gyrotropy of gyrating downstream ion distributions, which was later confirmed by hybrid simulations and detailed observations (Balikhin *et al.* 2008; Ofman *et al.* 2009; Pope, Gedalin & Balikhin 2019). As another example, the influence of α-particles on the shock structure was first elucidated using the test particle analysis and later supported by simulations (Gedalin 2017, 2019; Ofman *et al.* 2019). Test particle analysis has been used recently for studies of pickup ion acceleration at the shock front (Zirnstein *et al.* 2021). In the present study, we focus on the dependence of the direction and magnitude of the shift of a reflected particle along the shock front, without taking into account possible non-planarity or time dependence of the shock.

2. The model

We adopt a simple model including overshoot

$$B_{\rm bas} = \frac{R_{\rm bas}-1}{2} + \frac{R_{\rm bas}+1}{2}\tanh\frac{3x}{D}, \tag{2.1}$$

$$B_{\rm add} = R_{\rm add}\left(1-\tanh\frac{3(x-c_r)}{w_r}\right)\left(1+\tanh\frac{3(x-c_l)}{w_l}\right), \tag{2.2}$$

$$B = B_{\rm bas} + B_{\rm add}, \tag{2.3}$$

$$B_x = \cos\theta_{Bn}, \tag{2.4}$$

$$B_z = B\sin\theta_{Bn}, \tag{2.5}$$

$$B_y = k_B\left(\frac{{\rm d}B}{{\rm d}x}\right), \tag{2.6}$$

$$E_x = -k_E\left(\frac{{\rm d}B}{{\rm d}x}\right), \tag{2.7}$$

$$E_y = \sin\theta_{Bn}. \tag{2.8}$$

$$E_z = 0. \tag{2.9}$$

Here, the magnetic field is normalized on the upstream magnetic field B_u. All coordinates and lengths are normalized on the upstream convective gyroradius, V_u/Ω_u, where V_u is the plasma speed in NIF, and $\Omega_u = eB_u/m_pc$ is the upstream proton gyrofrequency, where e is the proton charge and m_p is the proton mass. The related upstream ion inertial length is c/ω_{pi}, where $\omega_{pi} = \sqrt{4\pi e^2 n_u/m_p}$ is the upstream proton plasma frequency, and n_u is the upstream proton number density. The Alfvénic Mach number is defined as usual, $M_A = V_u/v_A$, where the Alfvén speed is $v_A = B_u/\sqrt{4\pi n_u m_p}$. In the above expressions the angle θ_{Bn} between the shock normal and the upstream magnetic field is used. The expression (2.1) describes a monotonic increase of the main magnetic field, B_z, across the shock front, while (2.2) adds an overshoot. The magnetic compression is given by

$$\frac{B_d}{B_u} = \sqrt{R^2\sin^2\theta_{Bn} + \cos^2\theta_{Bn}}. \tag{2.10}$$

The relation of the non-coplanar component B_y approximately follows the theoretical analysis (Gedalin 1998) and was successfully applied to observational analysis (Gedalin *et al.* 2022). The electric field is normalized on V_uB_u/c. The coefficients k_E and k_B are

https://doi.org/10.1017/S0022377823000831 Published online by Cambridge University Press

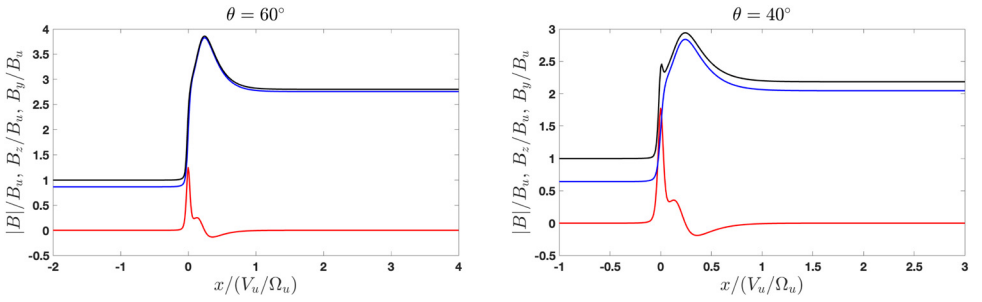

FIGURE 2. The components of the magnetic field and the magnetic field magnitude, according to the model: B_z (blue), B_y (red) and $|\boldsymbol{B}|$ (black). The component B_x is constant and not shown.

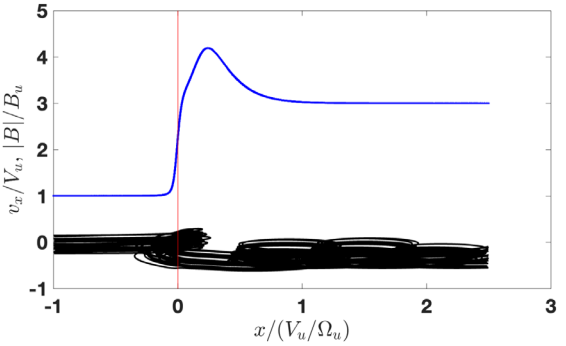

FIGURE 3. Black: x vs v_x for the reflected ions only. Blue: the magnetic field magnitude. The shock angle is $\theta_{Bn} = 75°$. Red line marks the position for which the cuts are presented.

found from the condition on the cross-shock potential

$$-\int E_x \,\mathrm{d}x = \phi_{\mathrm{NIF}} \equiv s_{\mathrm{NIF}}(m_p V_u^2/2e), \tag{2.11}$$

$$-\int (E_x + V_u \tan\theta_{Bn} B_y/c)\,\mathrm{d}x = \phi_{\mathrm{HT}} \equiv s_{\mathrm{HT}}(m_p V_u^2/2e). \tag{2.12}$$

The subscript HT means de Hoffman–Teller frame, which is the shock frame where the upstream plasma flow is along the upstream magnetic field. The parameters θ_{Bn}, B_d/B_u, R_{add}, s_{NIF}, s_{HT}, D, c_l, c_r, w_l and w_r completely define the planar stationary shock profile used in the analysis. In the present study we fix the following parameters: $M_A = 6$, $B_d/B_u = 3$, $R_{\mathrm{add}} = 1$, $s_{\mathrm{NIF}} = 0.4$, $s_{\mathrm{HT}} = 0.1$, $D = 2/M$, $w_l = D$, $w_r = 3D$, $c_l = 0.5D$, $c_r = 0.5D$. The incident ion distribution is Maxwellian with $\beta_i = 8\pi n_u T_{iu}/B_u^2 = 1$. The shock angle is varied. Figure 2 illustrates the magnetic field given by (2.1)–(2.6), for the same B_d/B_u, R_{add} and D, for two different shock angles, $\theta_{Bn} = 60°$ (a quasi-perpendicular shock) and $\theta_{Bn} = 40°$ (a quasi-parallel shock). In the quasi-parallel shock the non-coplanar component B_y is significant and even becomes larger than B_z in a small region, which results in the appearance of a small peak inside the ramp on the profile of the magnetic field magnitude. Ions are not sensitive to such small details of the shock profile.

https://doi.org/10.1017/S0022377823000831 Published online by Cambridge University Press

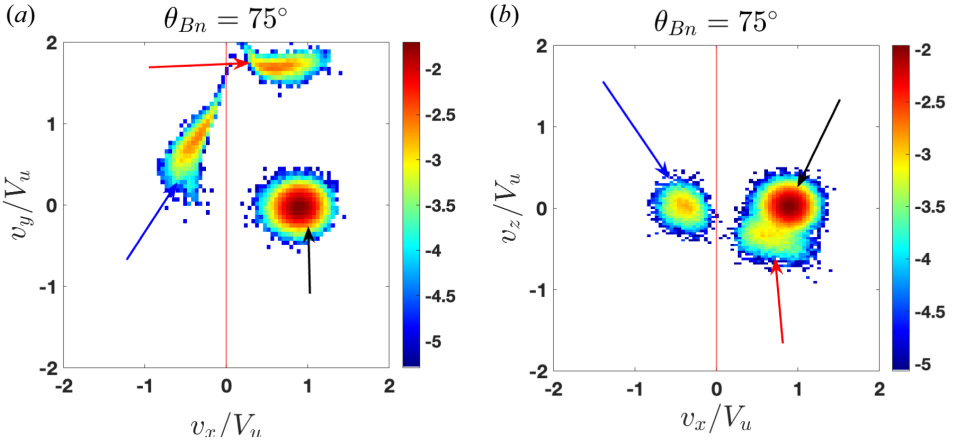

FIGURE 4. Two-dimensional cuts of the ion distribution at the red line position for $\theta_{Bn} = 75°$. (*a*) The reduced two-dimensional distribution function $f(v_x, v_y, x = 0)$. (*b*) The reduced two-dimensional distribution function $f(v_x, v_z, x = 0)$. The black arrow points to the directly transmitted ions. The blue arrow indicates the ions which are being reflected. The red arrow shows the reflected–transmitted ions.

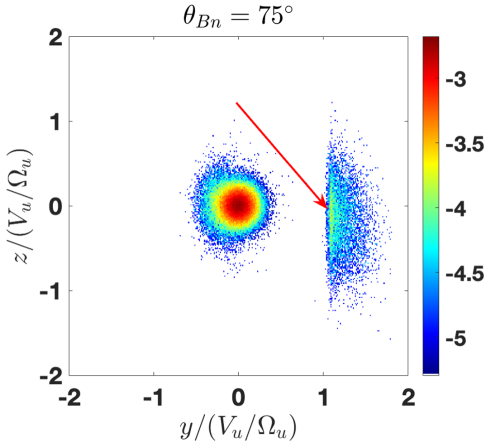

FIGURE 5. The y and z-coordinates of the ions crossing the red line position for $\theta_{Bn} = 75°$. The red arrow points to the population of the reflected–transmitted ions. The directly transmitted and reflected ions overlap on this plot.

3. Results

We trace 320 000 initially Maxwellian distributed ions across the shock by solving the equations of motion in the model fields. Figure 3 shows x vs v_x for reflected ions only, together with the magnetic field magnitude, for $\theta_{Bn} = 75°$. The red line marks the coordinate $x = 0$ at which the distributions shown below are derived. Note that the ions are reflected after the ramp but before the maximum of the overshoot. This means that the reflection is due to the combined effect of the deceleration by the cross-shock electric field and deflection by the increasing magnetic field (Gedalin *et al.* 2023).

Figure 4 shows two-dimensional cuts, $v_x - v_y$ and $v_x - v_z$, of the three-dimensional distribution function of all ions crossing the position $x = 0$ in any direction. The black

https://doi.org/10.1017/S0022377823000831 Published online by Cambridge University Press

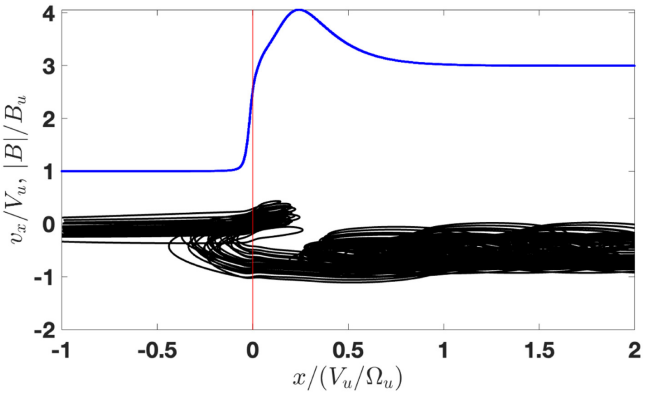

FIGURE 6. Black: x vs v_x for the reflected ions only. Blue: the magnetic field magnitude. The shock angle is $\theta_{Bn} = 60^\circ$. Red line marks the position for which the cuts are presented.

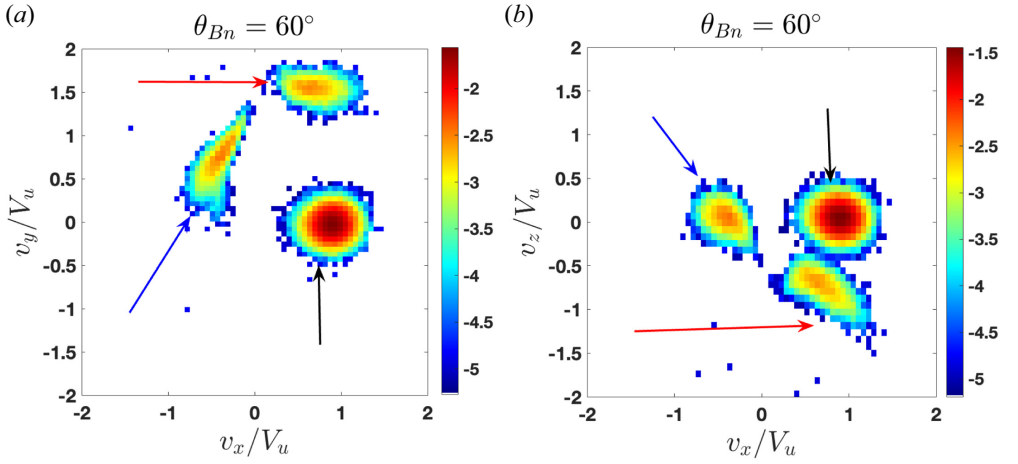

FIGURE 7. Two-dimensional cuts of the ion distribution at the red line position for $\theta_{Bn} = 60^\circ$. (*a*) The reduced two-dimensional distribution function $f(v_x, v_y, x = 0)$. (*b*) The reduced two-dimensional distribution function $f(v_x, v_z, x = 0)$. The black arrow points to the directly transmitted ions. The blue arrow indicates the ions which are being reflected. The red arrow shows the reflected–transmitted ions.

arrow marks the population of directly transmitted ions. The blue arrow marks the ions which are reflected, that is, move toward upstream at this position. The red arrow marks the reflected–transmitted ions, that is, the ions which were reflected, gyrated in the upstream and are crossing again the shock toward downstream. In the $v_x - v_y$ cut the three populations are clearly distinct, in the $v_x - v_z$ cut there is substantial overlap of directly transmitted and reflected–transmitted populations.

Figure 5 shows the y and z positions of the ions crossing the shock at $x = 0$. The reflected–transmitted ion population is significantly shifted along y, by one ion convective gyroradius and more, with a substantial dispersion of their z-coordinates.

Figure 6 shows x vs v_x for reflected ions only, together with the magnetic field magnitude, for $\theta_{Bn} = 60^\circ$, and it is rather similar to figure 3. Note that the magnetic field in the overshoot maximum is slightly smaller in this case. The left panel of figure 7 is

https://doi.org/10.1017/S0022377823000831 Published online by Cambridge University Press

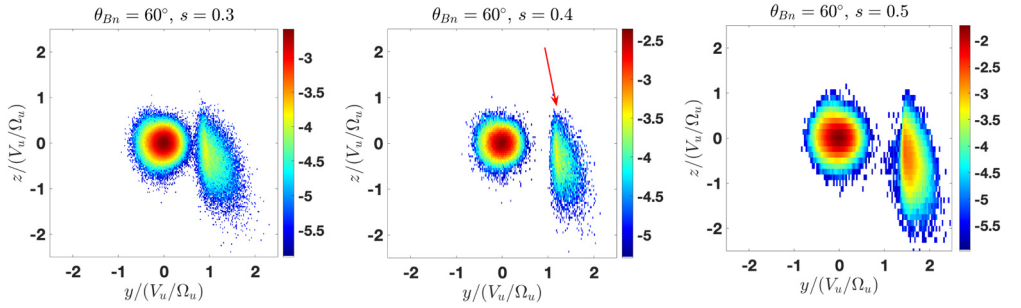

FIGURE 8. The y and z-coordinates of the ions crossing the red line position for $\theta_{Bn} = 60°$ and three different values of $s = 0.3, 0.4, 0.5$. The value of the cross-shock potential affects the dispersion of the positions but only weakly affects the position of the maximum.

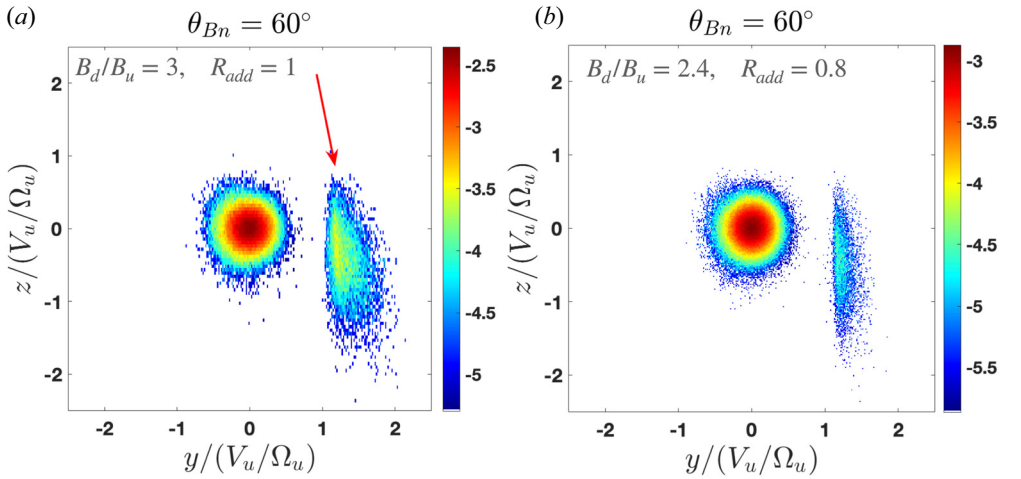

FIGURE 9. The y and z-coordinates of the ions crossing the red line position for $\theta_{Bn} = 60°$. Panel (a) corresponds to the basic set of parameters, $B_d/B_u = 3$ and $R_{\rm add} = 1$. Panel (b) corresponds to the reduced magnetic field, $B_d/B_u = 2.4$ and $R_{\rm add} = 0.8$. There are far fewer reflected ions for the lower magnetic field but the position of the maximum almost does not change.

similar to the left panel of figure 4. The right panel shows that reflected–transmitted ions acquire larger negative v_z for $\theta_{Bn} = 60°$ than for $\theta_{Bn} = 75°$. The three panels of figure 8 show y and z coordinates of ions crossing the plane $x = 0$, similarly to figure 5, but for three different values of the cross-shock potential, $s = 0.3, 0.4, 0.5$. The value of the cross-shock potential affects the dispersion of the positions but the position of the maximum is affected only weakly. This maximum is at $\Delta y \approx 1.2$, $\Delta z \approx -0.5$ for $s = 0.4$, so that the ions are moving at the angle $\approx 65°$ to the main magnetic field B_z. For larger s the maximum is slightly farther from the coordinate origin, for smaller s it is slightly closer. The z-coordinates of the reflected–transmitted ions experience a systematic shift toward negative values.

Figure 9 illustrates the effect of the magnetic compression and overshoot strength. For the lower magnetic field ion reflection is substantially weaker but the effect of the maximum of the position is not noticeable.

https://doi.org/10.1017/S0022377823000831 Published online by Cambridge University Press

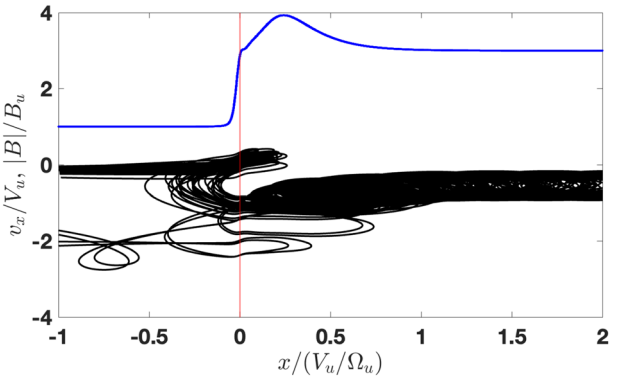

FIGURE 10. Black: x vs v_x for the reflected ions only. Blue: the magnetic field magnitude. The shock angle is $\theta_{Bn} = 50^\circ$. Red line marks the position for which the cuts are presented.

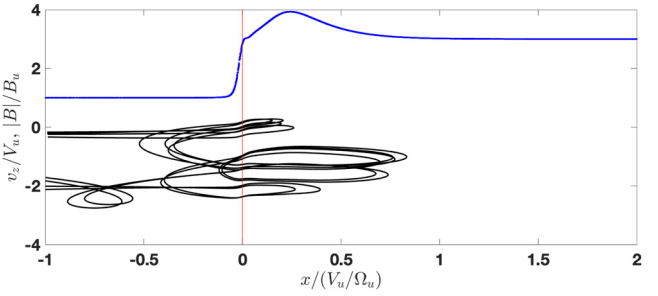

FIGURE 11. Black: $x - v_x$ for the multiply reflected ions only. Blue: the magnetic field magnitude. The shock angle is $\theta_{Bn} = 50^\circ$. Red line marks the position for which the cuts are presented.

In what follows we present the results of ion tracing in the model shock front for two smaller angles (Figures 10–17). The tracing procedure and the analysis are the same as for the two previous cases. The set of figures for $\theta_{Bn} = 50^\circ$ is similar to that for $\theta_{Bn} = 75^\circ$, while for $\theta_{Bn} = 40^\circ$ we show also the effects of s and B_d/B_u and $R_{\rm add}$, as is done above for $\theta_{Bn} = 60^\circ$. Variation of these parameters affects mainly the dispersion in the positions of the ions but only weakly affects the position of the maximum. There is further shift of the re-entry point in the z-direction. The major difference from the cases of larger angles is the appearance of backstreaming ions. These ions are produced by multiple reflection, as shown in figure 11. In all cuts these backstreaming ions are indicated with a green arrow. The number of backstreaming ions seems to increase with the decrease of the shock angle, at the expense of the reflected–transmitted ions.

Reduction of the magnetic field does not affect the position of the two maxima for $\theta_{Bn} = 40^\circ$. For $s = 0.4$ these maxima are at $\Delta y \approx 1.6$ and $\Delta z \approx -1.2$ for reflected–transmitted ions, and $\Delta y \approx 1.2$ and $\Delta z \approx -2.5$ for multiply reflected (backstreaming) ions. The maxima move closer to the coordinate origin for smaller s and farther from it for larger s. The angle between $\Delta \boldsymbol{r} = (\Delta y, \Delta z)$ and B_z is $\approx 53^\circ$.

4. Conclusions

Ion reflection at a collisionless shock front is a manifestly non-local process: the distance between the reflection point of an ion and the re-entry point of this ion into

https://doi.org/10.1017/S0022377823000831 Published online by Cambridge University Press

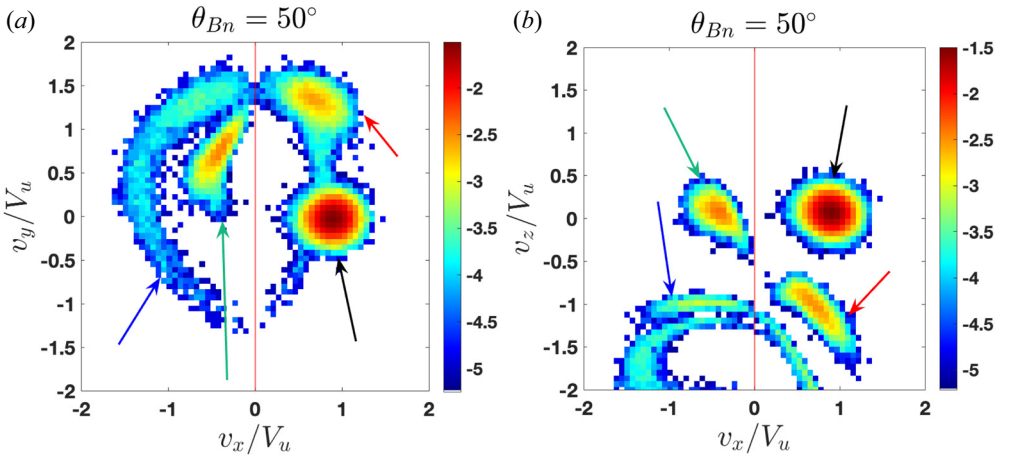

FIGURE 12. Two-dimensional cuts of the ion distribution at the red line position for $\theta_{Bn} = 50°$. (*a*) The reduced two-dimensional distribution function $f(v_x, v_y, x = 0)$. (*b*) The reduced two-dimensional distribution function $f(v_x, v_z, x = 0)$. The black arrow points to the directly transmitted ions. The blue arrow indicates the ions which are being reflected. The red arrow shows the reflected–transmitted ions. The green arrow points to the backstreaming ions.

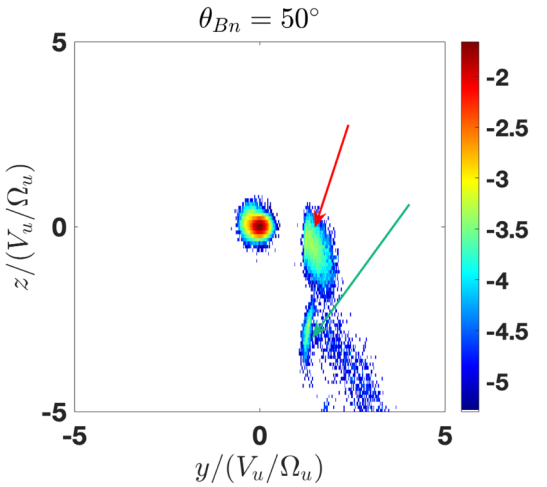

FIGURE 13. The y and z-coordinates of the ions crossing the red line position for $\theta_{Bn} = 50°$. The red arrow points to the reflected–transmitted ions. The green arrow points to the multiply reflected ions.

the shock transition is substantial and exceeds the upstream ion convective gyroradius. For quasi-perpendicular shocks the shift between the two points is mainly in the direction perpendicular to the magnetic field. For quasi-parallel shocks the shift in the perpendicular direction is similar to the shift in quasi-perpendicular shocks. It is accompanied by the shift in the direction opposite to the magnetic field direction. The latter parallel shift may significantly exceed the perpendicular shift. In a planar stationary shock this non-locality may seem of no importance because of the translational symmetry along the shock front. This is, however, not true. Increase of B_z ahead of the shock, the magnetic foot, is related to the current in the y-direction produced by the motion of reflected ions in this direction.

https://doi.org/10.1017/S0022377823000831 Published online by Cambridge University Press

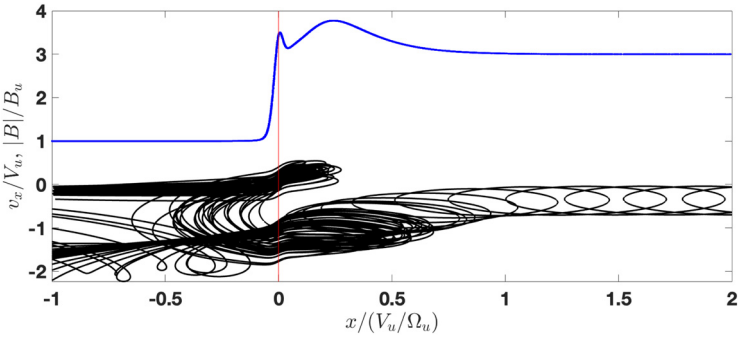

FIGURE 14. Black: x vs v_x for the reflected ions only. Blue: the magnetic field magnitude. The shock angle is $\theta_{Bn} = 40^\circ$. Red line marks the position for which the cuts are presented.

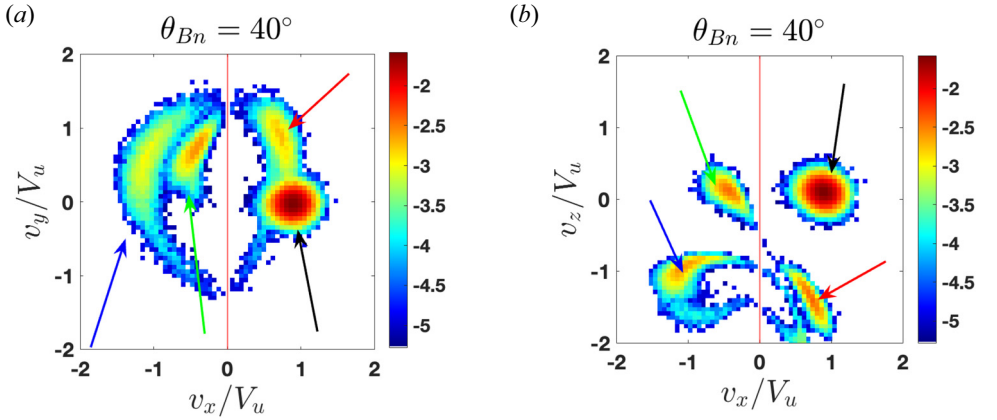

FIGURE 15. Two-dimensional cuts of the ion distribution at the red line position for $\theta_{Bn} = 40^\circ$. (*a*) The reduced two-dimensional distribution function $f(v_x, v_y, x = 0)$. (*b*) The reduced two-dimensional distribution function $f(v_x, v_z, x = 0)$. The black arrow points to the directly transmitted ions. The blue arrow indicates the ions which are being reflected. The red arrow shows the reflected–transmitted ions. The green arrow points to the backstreaming ions.

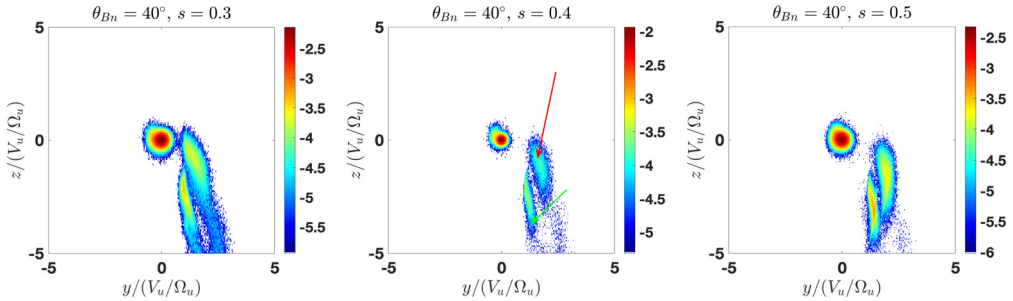

FIGURE 16. The y and z-coordinates of the ions crossing the red line position for $\theta_{Bn} = 40^\circ$ and three different values of $s = 0.3, 0.4, 0.5$. The value of the cross-shock potential affects the dispersion of the positions but only weakly affects the position of the maximum. The red arrow points to the reflected–transmitted ions for which $v_x > 0$. The green arrow points to the multiply reflected ions for which $v_x < 0$.

https://doi.org/10.1017/S0022377823000831 Published online by Cambridge University Press

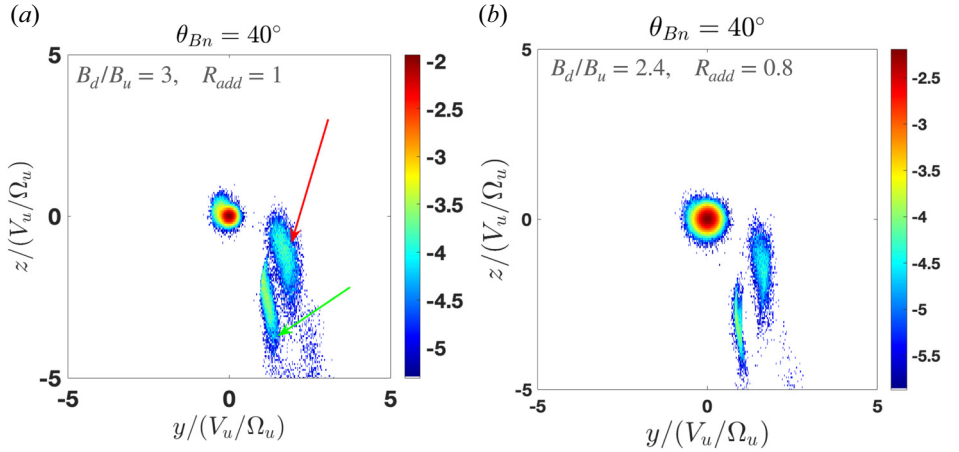

FIGURE 17. The y and z-coordinates of the ions crossing the red line position for $\theta_{Bn} = 40°$. Panel (a) corresponds to the basic set of parameters, $B_d/B_u = 3$ and $R_{\rm add} = 1$. Panel (b) corresponds to the reduced magnetic field, $B_d/B_u = 2.4$ and $R_{\rm add} = 0.8$. There are far fewer reflected ions for the lower magnetic field but the position of the maximum almost does not change. The red arrow points to the reflected–transmitted ions for which $v_x > 0$. The green arrow points to the multiply reflected ions for which $v_x < 0$.

For smaller shock angles the motion of reflected ions in the z-direction may become more substantial than in the y-direction, so that a current in the z-component is produced which should cause appearance of nonzero B_y in the foot.

Non-locality should be taken into account when interpreting observations. In multi-spacecraft missions different probes often observed different magnetic profiles. Distributions of reflected ions measured by a probe may have been produced at a shock crossing with parameters different from those at the measurement position.

Non-locality may be related to the development of rippling since a perturbation at one site is conveyed along the shock front by the reflected ions. If, for example, an overshoot increases at some site, ion reflection is enhanced at this site (Gedalin *et al.* 2023). A larger number of reflected ions enter the shock at a certain distance from the perturbed site. Higher ion pressure there would cause decrease of the overshoot, because of the momentum conservation, that is, the pressure balance. At this stage we are unable to quantify this possible instability. However, if it occurs, we can estimate the velocity of ripples as $\boldsymbol{V}_{\rm ripple} \sim \Omega\Delta\boldsymbol{r}/\pi$, where $\Delta\boldsymbol{r}$ is the vector from the reflection point to the re-entry point of the reflected–transmitted ions and we estimate that this motion occurs roughly during half of the upstream gyroperiod, π/Ω_u. The latter gives an estimate of the surface wave (rippling) period. Accordingly, the wavelength may be estimated as $\sim |\Delta\boldsymbol{r}|$. For our $\theta_{Bn} = 60°$ case this estimate gives $V_{\rm ripple} \approx 0.4V_u$ at $\approx 65°$ to B_z. For the $\theta_{Bn} = 40°$ case we have $V_{\rm ripple} \approx 0.65V_u$ at $\approx 53°$ to B_z.

Johlander *et al.* (2016) report MMS observations of a rippled shock with $\theta_{Bn} = 83°$ and $M = 4.2$. The rippling wavelength was estimated as $\approx V_u/\Omega_u$ (one in our dimensionless units) and the speed was estimated as $\sim 0.3V_u$. The propagation angle could not be determined. Burgess *et al.* (2016) performed three-dimensional hybrid simulations of a rippled shock. Although their analysis was devoted to the waves in the foot, the figures there show that the wavelength of ripples is $\sim V_u/\Omega_u$. The speed was estimated as $\sim 0.5V_u$. Our estimates of the speed and wavelength are in better agreement with the values found in observations (Johlander *et al.* 2016) and three-dimensional hybrid

https://doi.org/10.1017/S0022377823000831 Published online by Cambridge University Press

simulations (Burgess *et al.* 2016) than could be hoped for by the planar stationary model. Further comparison requires development of a more sophisticated model which would include rippling (Gedalin & Ganushkina 2022), and more three-dimensional simulations. Since the direction of the reflected ion motion is neither perpendicular nor parallel to the upstream magnetic field, two-dimensional simulations with the field in-plane or out-of-plane may suppress rippling or misestimate the rippling parameters. This has been shown in the comparison of two- and three-dimensional hybrid similations (Burgess *et al.* 2016), where it is found that fluctuations carried by the reflected ions are coupled to fluctuations propagating along the magnetic field. Non-locality of the reflection process may be directly related to the cross-field component of the rippling. The coupling with the other component may arise due to the developing rippling which causes variation of the shock angle along the shock front. Even initially perpendicular shocks become locally oblique (Burgess *et al.* 2016), so that the shift acquires component along the magnetic field. This issue is beyond the scope of this study and will be investigated separately.

In the cases $\theta_{Bn} = 50^\circ$ and $\theta_{Bn} = 40^\circ$ there appears a population of multiply reflected ions which eventually escape upstream. As long as the number of these ions is small relative to the number of the reflected–transmitted ions, the effect of the multiply reflected ions can be expected to be minor. With further decrease of the shock angle they may become progressively more important. If rippling is indeed related to the vector of the shift of reflected ions from the reflection point to the point of the re-entry into the shock, these ions may affect the rippling pattern by adding another wavelength or making the surface wave a wavepacket rather than a quasi-monochromatic wave. However, the main effect of the backstreaming ions may be causing instabilities ahead of the shock. Generated waves may drift toward the shock and interact with it, thus providing another mechanism of rippling generation (Hao *et al.* 2016). Shocks, which are strongly affected by waves excited due to backstreaming ions, are not within the scope of the present study.

Acknowledgements

Editor Antoine C. Bret thanks the referees for their advice in evaluating this article.

Funding

The work was partially supported by the European Union's Horizon 2020 research and innovation programme under grant agreement No 101004131 (SHARP). Wavelab850 software has been used for wavelet denoising.

Declaration of interests

The author reports no conflict of interest.

REFERENCES

Bale, S.D., Balikhin, M.A., Horbury, T.S., Krasnoselskikh, V.V., Kucharek, H., Möbius, E., Walker, S.N., Balogh, A., Burgess, D., Lembège, B., *et al.* 2005 Quasi-perpendicular shock structure and processes. *Space Sci. Rev.* **118** (1), 161–203.

Balikhin, M. & Gedalin, M. 2022 Collisionless shocks in the heliosphere: foot width revisited. *Astrophys. J.* **925** (1), 90.

Balikhin, M.A., Zhang, T.L., Gedalin, M., Ganushkina, N.Y. & Pope, S.A. 2008 Venus Express observes a new type of shock with pure kinematic relaxation. *Geophys. Res. Lett.* **35** (1), L01103.

Burgess, D., Hellinger, P., Gingell, I. & Trávníček, P.M. 2016 Microstructure in two- and three-dimensional hybrid simulations of perpendicular collisionless shocks. *J. Plasma Phys.* **82** (4), 905820401.

https://doi.org/10.1017/S0022377823000831 Published online by Cambridge University Press

Burgess, D., Lucek, E.A., Scholer, M., Bale, S.D., Balikhin, M.A., Balogh, A., Horbury, T.S., Krasnoselskikh, V.V., Kucharek, H., Lembège, B., *et al.* 2005 Quasi-parallel shock structure and processes. *Space Sci. Rev*. **118** (1), 205–222.

Burgess, D. & Scholer, M. 2007 Shock front instability associated with reflected ions at the perpendicular shock. *Phys. Plasmas* **14** (1), 012108.

Burgess, D., Wilkinson, W.P. & Schwartz, S.J. 1989 Ion distributions and thermalization at perpendicular and quasi-perpendicular supercritical collisionless shocks. *J. Geophys. Res*. **94**, 8783.

Cohen, I.J., Schwartz, S.J., Goodrich, K.A., Ahmadi, N., Ergun, R.E., Fuselier, S.A., Desai, M.I., Christian, E.R., McComas, D.J., Zank, G.P., *et al.* 2019 High-resolution measurements of the cross-shock potential, ion reflection, and electron heating at an interplanetary shock by MMS. *J. Geophys. Res*. **90** (A12), 12095.

Dimmock, A.P., Balikhin, M.A., Krasnoselskikh, V.V., Walker, S.N., Bale, S.D. & Hobara, Y. 2012 A statistical study of the cross-shock electric potential at low Mach number, quasi-perpendicular bow shock crossings using Cluster data. *J. Geophys. Res*. **117** (A), 02210.

Formisano, V. 1982 Measurement of the potential drop across the Earth's collisionless bow shock. *Geophys. Res. Lett*. **9**, 1033.

Gedalin, M. 1996 Ion reflection at the shock front revisited. *J. Geophys. Res*. **101** (A), 4871–4878.

Gedalin, M. 1997 Ion heating in oblique low-Mach number shocks. *Geophys. Res. Lett*. **24** (2), 2511–2514.

Gedalin, M. 1998 Low-frequency nonlinear stationary waves and fast shocks: hydrodynamical description. *Phys. Plasmas* **5** (1), 127–132.

Gedalin, M. 2016 Transmitted, reflected, quasi-reflected, and multiply reflected ions in low-Mach number shocks. *J. Geophys. Res*. **121** (1), 10.

Gedalin, M. 2017 Effect of alpha particles on the shock structure. *J. Geophys. Res*. **122** (1), 71–76.

Gedalin, M. 2019 Kinematic collisionless relaxation and time dependence of supercritical shocks with alpha particles. *Astrophys. J*. **880** (2), 140.

Gedalin, M. 2021 Shock heating of directly transmitted ions. *Astrophys. J*. **912** (2), 82.

Gedalin, M., Dimmock, A.P., Russell, C.T., Pogorelov, N.V. & Roytershteyn, V. 2023 Role of the overshoot in the shock self-organization. *J. Plasma Phys*. **89** (2), 905890201.

Gedalin, M., Friedman, Y. & Balikhin, M. 2015 Collisionless relaxation of downstream ion distributions in low-Mach number shocks. *Phys. Plasmas* **22** (7), 072301.

Gedalin, M. & Ganushkina, N. 2022 Implications of weak rippling of the shock ramp on the pattern of the electromagnetic field and ion distributions. *J. Plasma Phys*. **88** (3), 905880301.

Gedalin, M., Golbraikh, E., Russell, C.T. & Dimmock, A.P. 2022 Theory helps observations: determination of the shock Mach number and scales from magnetic measurements. *Front. Phys*. **10**, 11.

Gingell, I., Schwartz, S.J., Burgess, D., Johlander, A., Russell, C.T., Burch, J.L., Ergun, R.E., Fuselier, S., Gershman, D.J., Giles, B.L., *et al.* 2017 MMS observations and hybrid simulations of surface ripples at a marginally quasi-parallel shock. *J. Geophys. Res*. **77** (16), 736–11017.

Gosling, J.T. & Thomsen, M.F. 1985 Specularly reflected ions, shock foot thicknesses, and shock velocity determinations in space. *J. Geophys. Res*. **90**, 9893–9896.

Gosling, J.T., Thomsen, M.F., Bame, S.J., Feldman, W.C., Paschmann, G. & Sckopke, N. 1982 Evidence for specularly reflected ions upstream from the quasi-parallel bow shock. *Geophys. Res. Lett*. **9**, 1333.

Hao, Y., Lu, Q., Gao, X. & Wang, S. 2016 Ion dynamics at a rippled quasi-parallel shock: 2D hybrid simulations. *Astrophys. J*. **823** (1), 7.

Johlander, A., Schwartz, S.J., Vaivads, A., Khotyaintsev, Y.V., Gingell, I., Peng, I.B., Markidis, S., Lindqvist, P.A., Ergun, R.E., Marklund, G.T., *et al.* 2016 Rippled quasiperpendicular shock observed by the magnetospheric multiscale spacecraft. *Phys. Rev. Lett*. **117** (16), 165101.

Johlander, A., Vaivads, A., Khotyaintsev, Y.V., Gingell, I., Schwartz, S.J., Giles, B.L., Torbert, R.B. & Russell, C.T. 2018 Shock ripples observed by the MMS spacecraft: ion reflection and dispersive properties. *Plasma Phys. Control. Fusion* **60** (12), 125006.

LALTI, A., KHOTYAINTSEV, Y.V., DIMMOCK, A.P., JOHLANDER, A., GRAHAM, D.B. & OLSHEVSKY, V. 2022 A database of MMS bow shock crossings compiled using machine learning. *J. Geophys. Res*. **127**, e2022JA030454.

LEROY, M.M., WINSKE, D., GOODRICH, C.C., WU, C.S. & PAPADOPOULOS, K. 1982 The structure of perpendicular bow shocks. *J. Geophys. Res*. **87** (A7), 5081–5094.

LOBZIN, V.V., KRASNOSELSKIKH, V.V., MUSATENKO, K. & DUDOK DE WIT, T. 2008 On nonstationarity and rippling of the quasiperpendicular zone of the Earth bow shock: cluster observations. *Ann. Geophys*. **26** (9), 2899–2910.

LOWE, R.E. & BURGESS, D. 2003 The properties and causes of rippling in quasi-perpendicular collisionless shock fronts. *Ann. Geophys*. **21** (3), 671–679.

MORSE, D.L. 1973 Electrostatic potential rise across perpendicular shocks. *Plasma Phys*. **15** (1), 1262–1264.

MOULLARD, O., BURGESS, D., HORBURY, T.S. & LUCEK, E.A. 2006 Ripples observed on the surface of the Earth's quasi-perpendicular bow shock. *J. Geophys. Res*. **111** (A), A09113.

OFMAN, L., BALIKHIN, M., RUSSELL, C.T. & GEDALIN, M. 2009 Collisionless relaxation of ion distributions downstream of laminar quasi-perpendicular shocks. *J. Geophys. Res*. **114** (A), 09106.

OFMAN, L. & GEDALIN, M. 2013 Rippled quasi-perpendicular collisionless shocks: local and global normals. *J. Geophys. Res*. **118** (1), 5999–6006.

OFMAN, L., KOVAL, A., WILSON III, L.B. & SZABO, A. 2019 Understanding the role of α particles in oblique heliospheric shock oscillations. *J. Geophys. Res*. **82** (4), 905820401.

OMIDI, N., DESAI, M., RUSSELL, C.T. & HOWES, G.G. 2021 High Mach number quasi-perpendicular shocks: spatial versus temporal structure. *J. Geophys. Res*. **126** (9), e2021JA029287.

POPE, S.A., GEDALIN, M. & BALIKHIN, M.A. 2019 The first direct observational confirmation of kinematic collisionless relaxation in very low Mach number shocks near the Earth. *J. Geophys. Res*. **165** (1), 3–15.

SCHWARTZ, S.J., DOUGLAS, F.T., THOMSEN, M.F. & FELDMAN, W.C. 1987 Electron dynamics and potential jump across slow mode shocks. *J. Geophys. Res*. **92**, 3165.

SCHWARTZ, S.J., THOMSEN, M.F., BAME, S.J. & STANSBERRY, J. 1988 Electron heating and the potential jump across fast mode shocks. *J. Geophys. Res*. **93** (A11), 12923–12931.

SCKOPKE, N., PASCHMANN, G., BAME, S.J., GOSLING, J.T. & RUSSELL, C.T. 1983 Evolution of ion distributions across the nearly perpendicular bow shock – Specularly and non-specularly reflected-gyrating ions. *J. Geophys. Res*. **88** (A8), 6121–6136.

SCKOPKE, N., PASCHMANN, G., BRINCA, A.L., CARLSON, C.W. & LUEHR, H. 1990 Ion thermalization in quasi-perpendicular shocks involving reflected ions. *J. Geophys. Res*. **95**, 6337.

SCUDDER, J.D., AGGSON, T., AGGSON, T.L., MANGENEY, A., LACOMBE, C. & HARVEY, C.C. 1986 The resolved layer of a collisionless, high beta, supercritical, quasi-perpendicular shock wave. I – Rankine–Hugoniot geometry, currents, and stationarity. *J. Geophys. Res*. **91** (A10), 11019–11052.

TRATTNER, K.J., FUSELIER, S.A., SCHWARTZ, S.J., KUCHAREK, H., BURCH, J.L., ERGUN, R.E., PETRINEC, S.M. & MADANIAN, H. 2023 Ion acceleration at the quasi-parallel shock: the source distributions of the diffuse ions. *J. Geophys. Res*. **128** (2), e2022JA030631.

WANG, R., VASKO, I.Y., ARTEMYEV, A.V., HOLLEY, L.C., KAMALETDINOV, S.R., LOTEKAR, A. & MOZER, F.S. 2022 Multisatellite observations of ion holes in the Earth's plasma sheet. *Geophys. Res. Lett*. **49** (8), e2022GL097919.

WOODS, L. 1971 On double-structured, perpendicular, magneto-plasma shock waves. *Plasma Phys*. **13**, 289–302.

ZANK, G.P., PAULS, H.L., CAIRNS, I.H. & WEBB, G.M. 1996 Interstellar pickup ions and quasi-perpendicular shocks: implications for the termination shock and interplanetary shocks. *J. Geophys. Res*. **101** (A), 457–478.

ZIRNSTEIN, E.J., KUMAR, R., BANDYOPADHYAY, R., DAYEH, M.A., HEERIKHUISEN, J. & MCCOMAS, D.J. 2021 Turbulent acceleration of interstellar pickup ions at the heliospheric termination shock forms the global ENA spectrum. *Astrophys. J. Lett*. **916** (2), L21.